International Journal of Automotive Technology, Vol. 21, No. 3, pp. 691−702 (2020)
DOI 10.1007/s12239−020−0067−y

pISSN 1229−9138/ eISSN 1976−3832

ESO-BASED TERMINAL SLIDING MODE CONTROL FOR UNCERTAIN FULL-CAR ACTIVE SUSPENSION SYSTEMS

Wang Gang*

School of Mechanical Engineering, Guizhou Institute of Technology, Guiyang 550003, China

(Received 30 October 2018; Revised 1 June 2019; Accepted 10 September 2019)

ABSTRACT−In this paper, a fault-tolerant-control (FTC) scheme with finite-time convergence characteristics for vehicle active suspension systems is proposed. A full-car model with unknown dynamics and uncertain parameters is studied. To stabilize the vertical, pitch, and roll displacements into a desired equilibrium in finite time with an uncertain mathematical model and actuator faults, a novel non-singular terminal sliding mode controller (NSTSMC) is designed to control the vertical, pitch, and roll displacements. The control scheme is absolutely continuous and robust. In addition, an improved extended state observer (IESO) with switch terms is employed to compensate for the lumped uncertainty in the suspension systems. Compared with the traditional feedback linearization control based on a linear extended state observer (LESO), this scheme can achieve higher control precision, especially for high-frequency road excitations. Finally, numerical results are shown to verify the merit and effectiveness of the proposed controller, where different types of road excitations are considered to verify the proposed approach in detail.

KEY WORDS : Fault tolerant control, Vehicle active suspensions, Terminal sliding mode, Finite-time control

1. INTRODUCTION

The suspension system is an essential component of an automobile that isolates the roughness of the road from being transmitted to the chassis of the automobile and ensures the safety of the driver (Youn *et al*., 2017). In general, traditional passive suspension systems have difficultly achieving satisfying performances. To further improve the ride comfort and maneuverability of the automobile, suspension systems with additional actuators have been widely studied, which include semi-active control (Karkoub and Zribi, 2006; Spelta *et al*., 2011; Unger *et al*., 2013; Brezas *et al*., 2015) and active control (Gosiewski and Mystkowski, 2008; Sande *et al*., 2013). Recently, the semi-active suspensions have been applied to most high-performance automobiles due to their low costs. Active suspension has not yet been popularized, but its development prospects have been much anticipated due to its performance advantages. To save the control cost of the active suspension, an energy-regenerative suspension system was studied by Zhang *et al*. (2012, 2015), and Huang *et al*. (2015a), and the basic concept of the scheme is to reduce the energy consumption of the actuator through the recovery of the vibrational and heat energy of the damping oil. Undoubtedly, with the development of low energy consumption and energy-regenerative systems, vehicle active suspension systems have a promising future.

Because of the complexity and the contradictions in the performances of suspension systems, study of advanced control strategies for automobile suspensions is an active area of research. The H_∞ control approaches were applied for the active control of automobile suspension systems (Gao *et al*., 2006; Akbari and Lohmann, 2010; Sun *et al*., 2011; Wang *et al*., 2015a, 2015b; Wang *et al*., 2019). In this approach, sprung acceleration is generally used as the controlled output to minimize the H_∞ norm in the presence of road surface disturbances. Since it is robust, this approach can also supply H_∞ performance of the system when actuator delays and faults occur. However, the H_∞ control method can only be used in linear time-invariant systems, and nonlinear terms are simplified into linear terms in the suspension modeling of the full-car, which makes the control scheme to achieve the desired objectives difficult. Therefore, nonlinear methods were proposed for nonlinear active suspensions, such as backstepping control (Yagiz and Hacioglu, 2008; Sun *et al*., 2013, 2014), adaptive sliding fault tolerant control (Liu *et al*., 2016), and fuzzy control (Lin and Lian, 2011).

In most of the abovementioned methods, a precise mathematical model is required. In the work presented by Sun *et al*. (2013, 2014), only the uncertainties of the sprung mass were considered. Taking into account the practical suspension system, there are still other unknown dynamics and external disturbances, and thus, use of the previous methods to ensure the stability of the system is difficult, and more state variables must be measured. A sliding-

**Corresponding author*. e-mail: 20170815@git.edu.cn

mode control scheme that was based on the disturbance observer was applied to the uncertain quarter-car suspension system (Deshpande *et al*., 2014). The research by Huang *et al*. (2015b) used an adaptive neural network to estimate the uncertainty of the quarter-car suspension, which could guarantee the boundedness of the closed-loop system. However, the design scheme was complex, a number of parameters needed to be tuned, and the error was not significantly reduced. Considering the disadvantages of the above methods, Pan *et al*. (2015a) proposed the LESO-based feedback linearization control for the uncertain quarter-car active suspension system, which applied a LESO to compensate for the lumped uncertainty of the system. The estimation error was reduced with the increase in bandwidth, achieving better control. LESOs as the core component of the active disturbance rejection control can process the internal and external dynamics of the system simultaneously, and they have been applied to many engineering practices (Zheng *et al*., 2009; Guo and Zhao, 2011; Boker and Khalil, 2013; Shao and Wang, 2014; Yao *et al*., 2014; Zhao and Guo, 2015; Ran *et al*., 2016; Ahmed and Chen, 2018), such as motor, aircraft, and automobile control. Although the traditional LESO can achieve good performances, the capability of the high-frequency disturbance rejection is poor and limited to the hardware equipment, the bandwidth parameter cannot be increased freely, and it is difficult to obtain a higher accuracy of the displacement control. Because the finite-time control technique (Hong, 2002; Hong *et al*., 2002; Zhang *et al*., 2013; Pan *et al*., 2015b; Xiong *et al*., 2015; Li *et al*., 2012; Wang *et al*., 2017) has a stronger disturbance rejection and a faster convergence performance, some special NESO structures were proposed by Guo and Zhao (2011) and Li *et al*. (2012), which further improved the performance for the observer. To make the observation error converge to zero in a finite time, a novel ESO with switching terms is proposed for the first time herein, inspired by the finite time control technique (Xiong *et al*., 2015), which exhibited a better disturbance rejection performance than the previous ESO by introducing switching terms of the output error.

To achieve a higher accuracy in the vehicle suspension active control, a FTC scheme based on an ESO is proposed in this paper. A complete vehicle suspension model is studied, since the studies on the uncertain full-car suspensions are relatively rare at present. The technological advantages of the scheme are as follow: no precise mathematical model is required, only a small number of sensors is needed, and the design process is simple. The advantages of the scheme are verified by simulations. This scheme exhibits a stronger high-frequency active disturbance rejection performance than the traditional LESO-based feedback linearization control under the same observation bandwidth, and the vertical, pitch, and roll displacements can converge to zero in finite time, effectively improving the comfort, maneuverability, and stability of the vehicle. The features of this study are as follows:

1) A finite-time FTC scheme based on an ESO is developed for uncertain full-car active suspension systems.
2) A novel NSTSMC technique is proposed to stabilize the heave, pitch and roll displacements in a given equilibrium in finite time.
3) The dependence on the model and the sensor requirement is reduced.
4) The finite-time stability of the suspension system is analyzed.

The paper is organized as follows. The model and the control problem are formulated in Section 2. The observer and controller designs are presented in Sections 3 and 4, respectively. Numerical results are provided in Section 5, and concluding remarks are given in Section 6.

2. PROBLEM FORMULATION

To capture the heave, pitch, and roll characteristics of a car body, a full-car model with an active suspension system is considered, as shown in Figure 1. In this model, the chassis mass is denoted by M and the mass moment of inertia for the roll and pitch displacements are denoted by I_x and I_{zz}, respectively, which are uncertain parameters. m_i (i = 1, 2, 3, 4) is the unsprung mass. y, θ, and ϕ denote the heave, pitch, and roll displacements, respectively. F_{di} is the damper force of the suspension system. F_{mi} is the damping force of the tire. F_{si} is the spring force of the suspension system. F_{ti} is the elasticity force of the tire. u_i is the active control input. y_i and y_{0i} denote the vertical displacements of the unsprung mass and road surface, respectively. a, b and c, d represent the horizontal and longitudinal distances from the suspensions to the center of the car body, respectively. The damping of the tires is omitted in most studies, but it is inherent in actual operations for preventing the continuous vibrations of the unprung mass.

Based on the Lagrange equations, the motion equations of the full-car model can be easily expressed as follows:

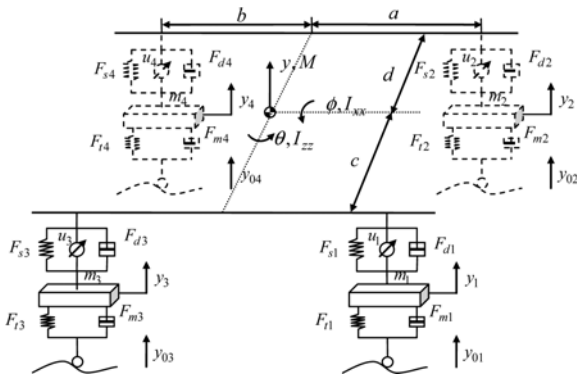

Figure 1. Full-car suspension model.

$$M\ddot{y}_u = -F_{d1} - F_{d2} - F_{d3} - F_{d4} - F_{s1} - F_{s2} - F_{s3} - F_{s4} + u_y \tag{1}$$

$$I_{zz}\ddot{\theta} = -\cos\theta \begin{bmatrix} a(F_{d1} + F_{d2} + F_{s1} + F_{s2}) \\ -b(F_{d3} + F_{d4} + F_{s3} + F_{s4}) \end{bmatrix} + u_\theta \tag{2}$$

$$I_{xx}\ddot{\phi} = -\cos\phi \begin{bmatrix} d(F_{d2} + F_{d4} + F_{s2} + F_{s4}) \\ -c(F_{d1} + F_{d3} + F_{s1} + F_{s3}) \end{bmatrix} + u_j \tag{3}$$

$$m_1\ddot{y}_1 = F_{d1} + F_{s1} - F_{t1} - F_{m1} - u_1 \tag{4}$$

$$m_2\ddot{y}_2 = F_{d2} + F_{s2} - F_{t2} - F_{m2} - u_2 \tag{5}$$

$$m_3\ddot{y}_3 = F_{d3} + F_{s3} - F_{t3} - F_{m3} - u_3 \tag{6}$$

$$m_4\ddot{y}_4 = F_{d4} + F_{s4} - F_{t4} - F_{m4} - u_4 \tag{7}$$

where

$$u_y = u_1 + u_2 + u_3 + u_4$$

$$u_\theta = a(u_1 + u_2) - b(u_3 + u_4)$$

$$u_j = d(u_2 + u_4) - c(u_1 + u_3)$$

Supposing that there are potential actuator faults, the real control forces can be expressed as

$$u_i = \lambda_i u_{ri},\ i = 1,2,3,4,\ \lambda_i \in (0,1] \tag{8}$$

where λ_i stands for the unknown fault rate, and u_{ri} is the ideal control law to be designed. If $\lambda_i = 0$, the actuators have completely failed and the system enters passive mode. $\lambda_i = 1$ means that the actuators are ideal. $\lambda_i \in (0, 1)$ indicates that the actuators have partial faults.

Note that the following relations are always true

$$\begin{aligned} &\lambda_1 u_{r1} + \lambda_2 u_{r2} + \lambda_3 u_{r3} + \lambda_4 u_{r4} \\ &= \delta_y (u_{r1} + u_{r2} + u_{r3} + u_{r4}) + T_y \\ &a(\lambda_1 u_{r1} + \lambda_2 u_{r2}) - b(\lambda_3 u_{r3} + \lambda_4 u_{r4}) \\ &= \delta_\theta \left[a(u_{r1} + u_{r2}) - b(u_{r3} + u_{r4}) \right] + T_\theta \\ &d(\lambda_2 u_{r2} + \lambda_4 u_{r4}) - c(\lambda_1 u_{r1} + \lambda_3 u_{r3}) \\ &= \delta_j \left[d(u_{r2} + u_{r4}) - c(u_{r1} + u_{r3}) \right] + T_j \end{aligned} \tag{9}$$

where δ_y, δ_θ, δ_ϕ, T_y, T_θ, and T_ϕ are unknown time-varying parameters.

Letting

$$u_{ry} = u_{r1} + u_{r2} + u_{r3} + u_{r4}$$

$$u_{r\theta} = a(u_{r1} + u_{r2}) - b(u_{r3} + u_{r4})$$

$$u_{rj} = d(u_{r2} + u_{r4}) - c(u_{r1} + u_{r3})$$

then the real resultant forces can be rewritten as

$$\begin{aligned} u_y &= \delta_y u_{ry} + T_y \\ u_\theta &= \delta_\theta u_{r\theta} + T_\theta \\ u_\phi &= \delta_\phi u_{r\phi} + T_\phi \end{aligned} \tag{10}$$

where u_{ry}, $u_{r\theta}$, and $u_{r\phi}$ denote the desired resultant forces to be designed.

In actual suspension systems, it is impossible to establish an accurate mathematical model, regardless of how advanced the parameter identification techniques are. The key feature of the proposed scheme is that it does not require an accurate mathematical model. The only required information is the nominal values of the chassis mass and the mass moment of inertia for the roll and pitch displacements, which are denoted by M_m, I_{zzm}, and I_{xxm}, respectively. Parameter uncertainties and unknown dynamics typically exist, and the stiffness and damping coefficients may be time-varying in some situations. The elasticity and damping forces can be linear or nonlinear in different regions, which means that the forces F_{si}, F_{di}, F_{ti}, and F_{mi} and the real values of M, I_{zz}, and I_{xx} are unknown in realistic cases. Therefore, it is necessary to consider an uncertain full-car suspension model.

The state variables are defined as follows:

$$\begin{aligned} x_1 &= y, & x_8 &= \dot{y}_1 \\ x_2 &= \dot{y}, & x_9 &= y_2 \\ x_3 &= \theta, & x_{10} &= \dot{y}_2 \\ x_4 &= \dot{\theta}, & x_{11} &= y_3 \\ x_5 &= \phi, & x_{12} &= \dot{y}_3 \\ x_6 &= \dot{\phi}, & x_{13} &= y_4 \\ x_7 &= y_1, & x_{14} &= \dot{y}_4 \end{aligned} \tag{11}$$

The state-space equations of the full-car model can be written as

$$\begin{cases} \dot{x}_1 = x_2 \\ \dot{x}_2 = f_1 + b_1 u_{ry} \end{cases} \tag{12}$$

$$\begin{cases} \dot{x}_3 = x_4 \\ \dot{x}_4 = f_2 + b_2 u_{r\theta} \end{cases} \tag{13}$$

$$\begin{cases} \dot{x}_5 = x_6 \\ \dot{x}_6 = f_3 + b_3 u_{r\phi} \end{cases} \tag{14}$$

$$\begin{cases} \dot{x}_7 = x_8 \\ \dot{x}_8 = \dfrac{1}{m_1}(F_{d_1} + F_{s1} - F_{t1} - F_{m1}) - \dfrac{1}{m_1}u_1 \end{cases} \tag{15}$$

$$\begin{cases} \dot{x}_9 = x_{10} \\ \dot{x}_{10} = \dfrac{1}{m_2}(F_{d_2} + F_{s2} - F_{t2} - F_{m2}) - \dfrac{1}{m_2}u_2 \end{cases} \tag{16}$$

$$\begin{cases} \dot{x}_{11} = m x_{12} \\ \dot{x}_{12} = \dfrac{1}{m_3}(F_{d_3} + F_{s3} - F_{t3} - F_{m3}) - \dfrac{1}{m_3}u_3 \end{cases} \tag{17}$$

$$\begin{cases} \dot{x}_{13} = x_{14} \\ \dot{x}_{14} = \dfrac{1}{m_4}(F_{d4} + F_{s4} - F_{t4} - F_{m4}) - \dfrac{1}{m_4}u_4 \end{cases} \tag{18}$$

where

$$f_1 = -\frac{1}{M}\begin{pmatrix} F_{d1}+F_{d2}+F_{d3}+F_{d4} \\ +F_{s1}+F_{s2}+F_{s3}+F_{s4} \end{pmatrix} + \left(\frac{\delta_y}{M}-b_1\right)u_{ry}+\frac{T_y}{M}$$

$$f_2 = -\frac{1}{I_{zz}}\cos\theta\begin{bmatrix} a(F_{d1}+F_{d2}+F_{s1}+F_{s2}) \\ -b(F_{d3}+F_{d4}+F_{s3}+F_{s4}) \end{bmatrix} + \left(\frac{\delta_\theta}{I_{zz}}-b_2\right)u_{r\theta}+\frac{T_\theta}{I_{zz}}$$

$$f_3 = -\frac{1}{I_{xx}}\cos\phi\begin{bmatrix} d(F_{d2}+F_{d4}+F_{s2}+F_{s4}) \\ -c(F_{d1}+F_{d3}+F_{s1}+F_{s3}) \end{bmatrix} + \left(\frac{\delta_\phi}{I_{xx}}-b_3\right)u_{r\phi}+\frac{T_\phi}{I_{xx}}$$

with

$$b_1=\frac{1}{M_m},\ b_2=\frac{1}{I_{zzm}},\ \text{and}\ b_3=\frac{1}{I_{xxm}}$$

In the above equations, f_1, f_2, and f_3 consist of uncertain parameters, unknown internal dynamics, and unknown fault rates. Thus, they are regarded as the lumped uncertainties of the systems in this study. The main control objectives can be summarized as follows:

(i) *Finite-time stabilization:* A control strategy must be synthesized such that the heave, pitch, and roll displacements of the vehicle body converge to a given equilibrium in finite time to improve ride comfort, handling, and stability in the presence of an uncertain plant model and actuator faults. In addition, all the lumped uncertainties should be compensated for by employing an improved ESO in real time.

(ii) *Suspension movement limitation:* Limited by the mechanical structure, the suspension space must be preserved to avoid damaging the actuator and other mechanical structure. Defining the maximum suspension travel as Δy_{max}, the requirements can be formulated as

$$|\Delta y_i| \le \Delta y_{max},\ i = 1, 2, 3, 4 \tag{19}$$

where

$$\Delta y_1 = y + a\sin\theta - c\sin\phi - y_1$$

$$\Delta y_2 = y + a\sin\theta + d\sin\phi - y_2$$

$$\Delta y_3 = y - b\sin\theta - c\sin\phi - y_3$$

$$\Delta y_4 = y - b\sin\theta + d\sin\phi - y_4$$

3. EXTENDED STATE OBSERVER DESIGN

To handle the uncertainties of the suspension systems in the controller design, three improved NESOs are employed to estimate the lumped uncertainties online. The lumped uncertainty's first time derivative is also considered as the augmented state to improve the control precision.

Assumption 1: The lumped uncertainties f_1, f_2, and f_3 are continuously differentiable and their second time derivatives are bounded for a given positive constant M, that is

$$|\ddot{f}_i| < M,\ i = 1, 2, 3 \tag{20}$$

This assumption is reasonable for vehicle active suspension systems. The mechanical structure and actuator do not allow the internal dynamics to change instantaneously, which implies that the lumped uncertainty is continuously differentiable and its second time derivative is bounded as well (Pan *et al*., 2015a).

First, an extended state observer for the lumped uncertainty f_1 is designed. Letting $x_{y1} = x_1$, $x_{y2} = x_2$, $x_{y3} = f_1$, and $x_{y4} = \dot{f}$, the second-order subsystem in Equation (12) can be extended to the following high-order subsystem

$$\begin{cases} \dot{x}_{y1} = x_{y2} \\ \dot{x}_{y2} = x_{y3} + b_1 u_y \\ \dot{x}_{y3} = x_{y4} \\ \dot{x}_{y4} = \ddot{f}_1 \end{cases} \tag{21}$$

where x_{y4} denotes the rate of change of f_1.

According to Guo and Zhao *et al*. (2014), a generalized ESO can be designed as follows

$$\begin{cases} \dot{\hat{x}}_{y1} = \hat{x}_{y2} + \omega_0^{-2} g_1(e_{y1}\omega_0^3) \\ \dot{\hat{x}}_{y2} = \hat{x}_{y3} + b_1 u_y + \omega_0^{-1} g_2(e_{y1}\omega_0^3) \\ \dot{\hat{x}}_{y3} = \hat{x}_{y4} + g_3(e_{y1}\omega_0^3) \\ \dot{\hat{x}}_{y4} = \omega_0 g_4(e_{y1}\omega_0^3) \end{cases} \tag{22}$$

where $\hat{x}_{yi}$ is the estimate of the state x_{yi}, $\omega_0 > 1$ is the bandwidth parameter, $e_{y1} = x_{y1} - \hat{x}_{y1}$, and $g_i(\cdot)$ is a function chosen by the designer.

The most important role of the ESO in Equation (22) is that the state of the observer $\hat{x}_{yi}$ can be considered as the estimate of the state of the original system x_{yi} by choosing appropriate functions $g_i(\cdot)$ and bandwidth parameter ω_0. The convergence of the estimate errors is described in the following theorem.

Theorem 1 (Guo and Zhao, 2011). Considering Equations (21) and (22) and supposing that Assumption 1 is satisfied, there exists a constant t_p such that

$$|e_{yi}| \le O\left(\frac{1}{\omega_0^{5-i}}\right),\ \forall t > t_p,\ i = 1,2,3,4.$$

Remark 1. From Theorem 1, the estimate error will converge to a residual set around zero with an increase in the bandwidth parameter. However, limited by hardware constraints (e.g., sampling rate, high frequency dynamics, and measurement noise), the bandwidth cannot be increased arbitrarily. To further improve the estimate performance with a limited bandwidth, a novel ESO is proposed in this paper.

Inspired by the work by Xiong *et al*. (2015), an improved NESO can be designed as follows

$$\begin{cases}\dot{\hat{x}}_{y1}=\hat{x}_{y2}+\omega_0^{-2}\lambda_1 fal_1+k_1\,\mathrm{sgn}(e_{y1})\\ \dot{\hat{x}}_{y2}=\hat{x}_{y3}+b_1u_y+\omega_0^{-1}\lambda_2 fal_2+k_2\,\mathrm{sgn}(e_{y1})\\ \dot{\hat{x}}_{y3}=\hat{x}_{y4}+\lambda_3 fal_3+k_3\,\mathrm{sgn}(e_{y1})\\ \dot{\hat{x}}_{y4}=\omega_0\lambda_4 fal_4+k_4\,\mathrm{sgn}(e_{y1})\end{cases} \tag{23}$$

where

$$\lambda_i=\frac{4!}{i!(4-i)!},\ i=1,2,3,4,\ k_i>0$$

$$fal_i=\begin{cases}\mathrm{sgn}(gy)\left|gy\right|^{\alpha_i}+\mathrm{sgn}(gy)\left|gy\right|^{\beta_i} & \text{for}\left|gy\right|>r\\ \dfrac{gy}{r^{1-\alpha_i}}+\dfrac{gy}{r^{1-\beta_i}} & \text{for}\left|gy\right|\le r\end{cases}$$

with

$$gy=e_{y1}\omega_0^3,\ \alpha_1\in\left(\tfrac{3}{4},1\right),\ \alpha_i=i\alpha_1-(i-1)$$

$$\beta_i=\beta_1+(i-1)(\alpha_1-1),\ \beta_1=1/\alpha_1$$

Theorem 2 (Xiong *et al*., 2015). Considering Equations (21) and (23) and supposing that Assumption 1 is satisfied, all the errors can converge to zero in finite time with a properly selected k_i.

Remark 2. The improved ESO is the combination of the NESO with the switching terms. The ESO obeys the principle of "small error, large gain, and large error, small gain." By setting $\alpha_1 = 1$ and neglecting the switching terms, Equation (23) reduces to the traditional LESO. As indicated in most previous work (Guo and Zhao, 2011; Li *et al*., 2012; Ran *et al*., 2016), the NESO exhibits better disturbance rejection performance than the LESO. Introducing the switching terms of the output error can further improve the observation performance.

Following a similar procedure, the ESO for the lumped uncertainty f_2 can be designed as follows:

$$\begin{cases}\dot{\hat{x}}_{\theta1}=\hat{x}_{\theta2}+\omega_0^{-2}\lambda_1 fal_1+k_1\,\mathrm{sgn}(e_{\theta1})\\ \dot{\hat{x}}_{\theta2}=\hat{x}_{\theta3}+b_1u_\theta+\omega_0^{-1}\lambda_2 fal_2+k_2\,\mathrm{sgn}(e_{\theta1})\\ \dot{\hat{x}}_{\theta3}=\hat{x}_{\theta4}+\lambda_3 fal_3+k_3\,\mathrm{sgn}(e_{\theta1})\\ \dot{\hat{x}}_{\theta4}=\omega_0\lambda_4 fal_4+k_4\,\mathrm{sgn}(e_{\theta1})\end{cases} \tag{24}$$

where

$$\lambda_i=\frac{4!}{i!(4-i)!},\ i=1,2,3,4,\ k_i>0$$

$$fal_i=\begin{cases}\mathrm{sgn}(g\theta)\left|g\theta\right|^{\alpha_i}+\mathrm{sgn}(g\theta)\left|g\theta\right|^{\beta_i} & \text{for}\left|g\theta\right|>r\\ \dfrac{g\theta}{r^{1-\alpha_i}}+\dfrac{g\theta}{r^{1-\beta_i}} & \text{for}\left|g\theta\right|\le r\end{cases}$$

with

$$g\theta=e_{\theta1}\omega_0^3,\ \alpha_1\in\left(\tfrac{3}{4},1\right),\ \alpha_i=i\alpha_1-(i-1)$$

$$\beta_i=\beta_1+(i-1)(\alpha_1-1),\ \beta_1=1/\alpha_1$$

The ESO for the lumped uncertainty f_3 can be given as

$$\begin{cases}\dot{\hat{x}}_{\phi1}=\hat{x}_{\phi2}+\omega_0^{-2}\lambda_1 fal_1+k_1\,\mathrm{sgn}(e_{\phi1})\\ \dot{\hat{x}}_{\phi2}=\hat{x}_{\phi3}+b_1u_y+\omega_0^{-1}\lambda_2 fal_2+k_2\,\mathrm{sgn}(e_{\phi1})\\ \dot{\hat{x}}_{\phi3}=\hat{x}_{\phi4}+\lambda_3 fal_3+k_3\,\mathrm{sgn}(e_{\phi1})\\ \dot{\hat{x}}_{\phi4}=\omega_0\lambda_4 fal_4+k_4\,\mathrm{sgn}(e_{\phi1})\end{cases} \tag{25}$$

where

$$\lambda_i=\frac{4!}{i!(4-i)!},\ i=1,2,3,4,\ k_i>0$$

$$fal_i=\begin{cases}\mathrm{sgn}(g\phi)\left|g\phi\right|^{\alpha_i}+\mathrm{sgn}(g\phi)\left|g\phi\right|^{\beta_i} & \text{for}\left|g\phi\right|>r\\ \dfrac{g\phi}{r^{1-\alpha_i}}+\dfrac{g\phi}{r^{1-\beta_i}} & \text{for}\left|g\phi\right|\le r\end{cases}$$

with

$$g\phi=e_{\phi1}\omega_0^3,\ \alpha_1\in\left(\tfrac{3}{4},1\right),\ \alpha_i=i\alpha_1-(i-1)$$

$$\beta_i=\beta_1+(i-1)(\alpha_1-1),\ \beta_1=1/\alpha_1$$

Remark 3. The chattering phenomenon may result in the deterioration of the control precision. Thus, the boundary layer function fal_i is used in the ESO design to prevent chattering from occurring, and the switching terms $k_i\,\mathrm{sgn}(\cdot)$ are replaced by the following saturation functions

$$k_i\,\mathrm{sat}(\cdot)=\begin{cases}k_i\,\mathrm{sgn}(\cdot) & \text{if}\left|(\cdot)\right|>\kappa\\ \dfrac{k_i(\cdot)}{\kappa} & \text{if}\left|(\cdot)\right|\le\kappa\end{cases} \tag{26}$$

4. CONTROL LAW SYNTHESIS

In this section, a NSTSMC scheme based on ESO is presented for uncertain full-car active suspensions to stabilize the heave, pitch, and roll displacements simultaneously. Firstly, a desired sliding surface for the heave displacement is selected, and the controller is designed such that the sliding motion is attainable.

Defining a desired trajectory for the heave displacement as y_d, the tracking error is $e = y - y_d$. The main objective is to synthesize a control law that induces the following behavior:

$$\lim_{t\to T}e(t)=\lim_{t\to T}\dot{e}(t)=\lim_{t\to T}\ddot{e}(t)=0 \tag{27}$$

where T denote a finite time.

Step 1: A novel non-singular terminal sliding mode for Equation (12) is proposed as follows:

$$\sigma_y=\ddot{e}+\int_0^t\begin{bmatrix}c_2\,\mathrm{sig}(\ddot{e})^{\gamma_3}+\\ c_2c_1^{\gamma_3}\,\mathrm{sig}(\mathrm{sig}(\dot{e})^{r_2}+c_0^{\gamma_2}e)^{\gamma_1}\end{bmatrix}\mathrm{d}t \tag{28}$$

where c_0, c_1, and c_2 are all positive constants, and

$\gamma_1=\dfrac{3-2\gamma}{\gamma}$, $\gamma_2=\gamma$, $\gamma_3=\dfrac{3-2\gamma}{2-\gamma}$, $\gamma\in\left(1,\dfrac{3}{2}\right)$.

The notation: $\mathrm{sig}(a)^{\mathrm{b}}=\mathrm{sgn}(a)\cdot|a|^{\mathrm{b}}$.

Step 2: The following continuous sliding mode control law is selected

$$u_{\mathrm{ry}}=\upsilon_{\mathrm{ry}}-b_1^{-1}(\hat{f}_1-\ddot{y}_{\mathrm{d}}) \tag{29}$$

with

$$\dot{\upsilon}_{\mathrm{ry}}=b_1^{-1}(u_{\mathrm{ryn}}+u_{\mathrm{rys}}) \tag{30}$$

$$u_{\mathrm{ryn}}=-c_2\,\mathrm{sig}(\ddot{e})^{\gamma_3}-c_2c_1^{\gamma_3}\,\mathrm{sig}(\mathrm{sig}(\dot{e})^{\mathrm{r}_2}+c_0^{\gamma_2}e)^{\gamma_1} \tag{31}$$

$$u_{\mathrm{rys}}=-(k\varepsilon+\eta)\,\mathrm{sgn}(\sigma_{\mathrm{y}}) \tag{32}$$

where k, ε, and η are all positive values and will be decided later, and $\hat{f}_1$ is the estimate of f_1, which can be obtained by the proposed ESO.

Theorem 3. Under the proposed sliding mode control law (29), the finite-time stability for the heave displacement is guaranteed if the switching gains are selected such that the sliding surface (28) converges to zero in finite time.

Proof. Substituting the control law (29) into (12) yields

$$\dot{x}_2=b_1\upsilon_{\mathrm{ry}}+\tilde{f}_1+\ddot{y}_{\mathrm{d}} \tag{33}$$

where $\tilde{f}_1=f_1-\hat{f}_1$ is the error estimate of the lumped uncertainty f_1.

From above analysis, we know that $\hat{f}_1$ can be obtained by the proposed ESO. Thus, we have $|\tilde{f}_1|=|e_{\mathrm{y}3}|$, $|\dot{\tilde{f}}_1|=|e_{\mathrm{y}4}|$.

It is assumed that $|e_{\mathrm{y}3}|\le l_{\mathrm{d}}$ and $|e_{\mathrm{y}4}|\le k_{\mathrm{d}}$, where $l_{\mathrm{d}}>0$ and $k_{\mathrm{d}}>0$. Taking the derivative of (33) results in $\dddot{x}_2=b_1\ddot{\upsilon}_{\mathrm{ry}}+\dot{\tilde{f}}_1+\dddot{y}_{\mathrm{d}}\Rightarrow\dddot{e}=b_1\ddot{\upsilon}_{\mathrm{ry}}+\dot{\tilde{f}}_1$. Using (30), we further have $\dddot{e}=u_{\mathrm{ryn}}+u_{\mathrm{rys}}+\dot{\tilde{f}}_1$.

Selecting a Lyapunov function as $V(\sigma_{\mathrm{y}})=\dfrac{1}{2}\sigma_{\mathrm{y}}^2$ and taking the derivative of it results in the following:

$$\begin{aligned}\dot{V}(\sigma_{\mathrm{y}})&=\sigma_{\mathrm{y}}\dot{\sigma}_{\mathrm{y}}\\&=\sigma_{\mathrm{y}}\begin{bmatrix}\dddot{e}+c_2\,\mathrm{sig}(\ddot{e})^{\gamma_3}+\\c_2c_1^{\gamma_3}\,\mathrm{sig}(\mathrm{sig}(\dot{e})^{\mathrm{r}_2}+c_0^{\gamma_2}e)^{\gamma_1}\end{bmatrix}\\&=\sigma_{\mathrm{y}}\left[u_{\mathrm{rys}}+\dot{\tilde{f}}_1\right]\le-\eta|\sigma_{\mathrm{y}}|-(k\varepsilon-|\dot{\tilde{f}}_1|)|\sigma_{\mathrm{y}}|\end{aligned} \tag{34}$$

If we choose $\varepsilon>k_{\mathrm{d}}$ and $k\ge1$, the following inequality is obtained:

$$\dot{V}(\sigma_{\mathrm{y}})\le-\eta|\sigma_{\mathrm{y}}|=-\sqrt{2}\eta V(\sigma_{\mathrm{y}})^{1/2}\le0 \tag{35}$$

It is noted that $\eta>0$. Therefore, the terminal sliding mode $\sigma_y=0$ is attainable after time $\dfrac{2V(0)^{1/2}}{\sqrt{2}\eta}$.

Remark 4. There is only one parameter that must be tuned, i.e., $(k\varepsilon+\eta)>|e_{\mathrm{y}4}|$. From the above analysis, we know that the estimate errors will converge to zero in finite time. However, noise is always present in practical applications, which means that the bounds of errors l_{d} and k_{d} can converge to a small residual set in finite time. Therefore, it is convenient to tune the switching gain $(k\varepsilon+\eta)$.

Once the sliding surface $\sigma_{\mathrm{y}}=\dot{\sigma}_{\mathrm{y}}=0$, Equation (32) shows that

$$\dot{\mathbf{e}}=\mathbf{R}(\mathbf{e}) \tag{36}$$

where

$\mathbf{e}=[e\quad\dot{e}\quad\ddot{e}]^{\mathbf{T}}$, $\mathbf{R}(\mathbf{e})=[R_1\quad R_2\quad R_3]^{\mathbf{T}}$

$R_1(e\quad\dot{e}\quad\ddot{e})=\dot{e}$, $R_2(e\quad\dot{e}\quad\ddot{e})=\ddot{e}$,

$R_3(e\quad\dot{e}\quad\ddot{e})=-c_2\,\mathrm{sig}(\ddot{e})^{\gamma_3}-c_2c_1^{\gamma_3}\,\mathrm{sig}(\mathrm{sig}(\dot{e})^{\mathrm{r}_2}+c_0^{\gamma_2}e)^{\gamma_1}$

Lemma 1 (Zhang *et al*., 2013). If Equation (36) is homogeneous with degree $\tau<0$, then the origin of the system is finite-time stable, that is $\mathbf{e}=(0\quad0\quad0)^{\mathbf{T}}$.

Applying the conditions $\gamma_1=\dfrac{3-2\gamma}{\gamma}$, $\gamma_2=\gamma$, $\gamma_3=\dfrac{3-2\gamma}{2-\gamma}$, and $\gamma\in\left(1,\dfrac{3}{2}\right)$, Equation (36) yields the following for any $\partial>0$ and $w>0$:

$$\begin{aligned}&R_1(\partial^{\mathrm{w}_1}e,\partial^{\mathrm{w}_2}\dot{e},\partial^{\mathrm{w}_3}\ddot{e})=\partial^{\mathrm{w}_2}\dot{e}=\partial^{\tau+\mathrm{w}_1}R_1(e\quad\dot{e}\quad\ddot{e})\\&R_2(\partial^{\mathrm{w}_1}e,\partial^{\mathrm{w}_2}\dot{e},\partial^{\mathrm{w}_3}\ddot{e})=\partial^{\mathrm{w}_3}\ddot{e}=\partial^{\tau+\mathrm{w}_2}R_2(e\quad\dot{e}\quad\ddot{e})\\&R_3(\partial^{\mathrm{w}_1}e,\partial^{\mathrm{w}_2}\dot{e},\partial^{\mathrm{w}_3}\ddot{e})=\partial^{\tau+\mathrm{w}_3}R_3(e\quad\dot{e}\quad\ddot{e})\end{aligned} \tag{37}$$

where $\tau=w_2(1-\gamma_2)<0$, $w_1=w_2\gamma_2$, $w_2=w$, and $w_3=w_2(2-\gamma_2)$.

Therefore, the error dynamic system (36) is homogeneous with degree $\tau<0$ and weights (w_1 w_2 w_3). According to Definitions 1–3 presented by Zhang *et al*. (2013), it is evident from Lemma 1 that the origin of the system is finite-time stable. This completes the proof.

According to a similar analysis, the sliding surface and control law for the pitch displacement are selected such that the origin of subsystem (13) is finite-time stable, where we select zero reference trajectories:

$$\sigma_\theta=\dot{x}_4+\int_0^{\mathrm{t}}\begin{bmatrix}c_2\,\mathrm{sig}(\dot{x}_4)^{\gamma_3}+\\c_2c_1^{\gamma_3}\,\mathrm{sig}(\mathrm{sig}(x_4)^{\gamma_2}+c_0^{\gamma_2}x_3)^{\gamma_1}\end{bmatrix}\mathrm{d}t \tag{38}$$

$$u_{\mathrm{r}\theta}=\upsilon_{\mathrm{r}\theta}-b_2^{-1}\hat{f}_2 \tag{39}$$

with

$$\dot{\upsilon}_{\mathrm{r}\theta}=b_2^{-1}(u_{\mathrm{r}\theta\mathrm{n}}+u_{\mathrm{r}\theta\mathrm{s}}) \tag{40}$$

$$u_{\mathrm{r}\theta\mathrm{n}}=-c_2\,\mathrm{sig}(\dot{x}_4)^{\gamma_3}-c_2c_1^{\gamma_3}\,\mathrm{sig}(\mathrm{sig}(x_4)^{\gamma_2}+c_0^{\gamma_2}x_3)^{\gamma_1} \tag{41}$$

$$u_{\mathrm{r}\theta\mathrm{s}}=-(k\varepsilon+\eta)\,\mathrm{sgn}(\sigma_\theta) \tag{42}$$

The sliding surface and control law for the roll displacements are selected as follows

$$\sigma_\phi=\dot{x}_6+\int_0^{\mathrm{t}}\begin{bmatrix}c_2\,\mathrm{sig}(\dot{x}_6)^{\gamma_3}+\\c_2c_1^{\gamma_3}\,\mathrm{sig}(\mathrm{sig}(x_6)^{\gamma_2}+c_0^{\gamma_2}x_5)^{\gamma_1}\end{bmatrix}\mathrm{d}t \tag{43}$$

$$u_{\mathrm{r}\phi}=\upsilon_{\mathrm{r}\phi}-b_3^{-1}\hat{f}_3 \tag{44}$$

with

$$\dot{\upsilon}_{r\phi} = b_3^{-1}(u_{r\phi n} + u_{r\phi s}) \tag{45}$$

$$u_{r\phi n} = -c_2 \operatorname{sig}(\dot{x}_6)^{\gamma_3} - c_2 c_1^{\gamma_3} \operatorname{sig}(\operatorname{sig}(x_6)^{\gamma_2} + c_0^{\gamma_2} x_5)^{\gamma_1} \tag{46}$$

$$u_{r\phi s} = -(k\varepsilon + \eta)\operatorname{sgn}(\sigma_\phi) \tag{47}$$

Remark 5. During implementation, the three sliding mode control laws are independent of each other, and u_y, u_θ, and u_ϕ control the displacements of the heave, pitch, and roll directions, respectively. This decentralized control manner is more tolerant to sensor failure. If the sensor of θ fails, there is no impact on the heave and roll displacements.

The control signals u_{ry}, $u_{r\theta}$, and $u_{r\phi}$ are the combination of the actual control input u_{ri}. There are infinite solutions since the number of inputs u_i is greater than the number of control signals. To obtain a set of feasible solutions, we add the constraint $u_{r3}c = u_{r4}d$, such that

$$u_{r1} = \frac{bdu_{ry} + du_{r\theta} - (a+b)u_{r\phi}}{(a+b)(c+d)}$$

$$u_{r2} = \frac{cbu_{ry} + cu_{r\theta} + (a+b)u_{r\phi}}{(a+b)(c+d)}$$

$$u_{r3} = \frac{d(au_{ry} - u_{r\phi})}{(a+b)(c+d)}$$

$$u_{r4} = \frac{c(au_{ry} - u_{r\theta})}{(a+b)(c+d)}$$

Remark 6. Since the actuator is placed between the chassis and the wheel in the active suspension systems, the suspension space must be preserved to avoid damaging the actuator and other mechanical structures when the vehicle is subject to uneven road. From the work by Yagiz and Hacioglu (2008), we know that if the reference trajectory is assigned as zero, the suspension working space may reach its working limits for the larger excitation. Thus, we define the following the desired trajectory for the heave displacement:

$$\begin{cases} y_d = y_c, & \text{for } |\Delta y_i| > \Delta y_{max} \\ y_d = 0, & \text{for } |\Delta y_i| \le \Delta y_{max} \end{cases}$$

where y_c represents the effective value of y_i under the center of gravity of the chassis, that is

$$y_c = \frac{b(dy_1 + cy_2) + a(dy_3 + cy_4)}{(a+b)(c+d)}.$$

5. SIMULATION RESULTS AND COMPARISON

In this section, the proposed ESO-based NCTSMC scheme is applied to the uncertain full-car suspension model shown in Figure 1. The traditional feedback linearization control based on a LESO proposed by Guo and Zhao (2011) is also compared to the simulations. The unknown dynamics are assumed to have the same form as those used by Yagiz and Hacioglu (2008):

$$F_{si} = k_i(\Delta y_i) + k_{ni}(\Delta y_i)^3 \tag{48}$$

$$F_{di} = b_{di}\Delta\dot{y}_i \tag{49}$$

$$F_{ti} = k_{ti}(y_i - y_{0i}) \tag{50}$$

$$F_{mi} = b_{mi}(\dot{y}_i - \dot{y}_{0i}) \tag{51}$$

where k_i and k_{ni} (i = 1, 2, 3, 4) are the stiffness coefficients of the suspension spring for the linear and cubic terms, b_{di} denotes the damping coefficient of the suspension damper, Δy_i is the change rate of Δy_i, k_{ti} and b_{mi} are the stiffness and damping coefficients of the tire, respectively.

The suspension parameters used by Yagiz and Hacioglu (2008) are adopted in this paper and are shown in Table 1. The controller and observer parameters are provided in Tables 2 and 3, respectively. All the initial states are set to zero so that the suspension model is established on a static position. It is assumed that the measurement noise is a zero mean Gaussian distributed random signal with 1×10^{-6}.

5.1. Simulation in Case 1 (No actuator faults)

In this case, we assume that the actuator is ideal, that is, λ_i

Table 1. Parameters of full-car model.

Parameter	Value	Parameter	Value
M	1000 kg	k_{ti}	250,000 N/m
I_{xx}	550 kgm^2	b_{mi}	1000 Ns/m
I_{zz}	1848 kgm^2	a	1.2 m
$m_1 = m_2$	25 kg	b	1.4 m
$m_3 = m_4$	45 kg	c	0.7 m
$k_1 = k_2$	15,000 N/m	d	0.8 m
$k_3 = k_{24}$	17,000 N/m	M_m	900 kg
$k_{n1} = k_{n2}$	150,000 N/m^3	I_{xxm}	500 kgm^2
$k_{n3} = k_{n4}$	170,000 N/m^3	I_{zzm}	1700 kgm^2
b_{di}	1500 Ns/m	Δy_{max}	0.08 m

Table 2. Controller design parameters.

Parameter	c_0	c_1	c_2	γ	$k\varepsilon + \eta$
Value	1	21	16	9/7	21

Table 3. Observer parameters.

Parameter	Value	Parameter	Value
ω_0	100	k_1	0.1
α_1	0.8	k_2	200
r	0.1	k_3	3 × 10
κ	1×10^{-5}	k_4	8×10^6

= 1 for i = 1, 2, 3, 4. A bump excitation is employed as the road disturbance y_{0i}, which can be described as follows:

$$y_{01}(t)=\begin{cases} b_0(1-\cos(2\pi Vt/l)), & 0\le t\le l/V \\ 0, & t>l/V \end{cases} \tag{52}$$

where b_0 = 0.1 m denotes the height of the bump, l = 5 m is the length of the bump, V = 15 m/s is the vehicle velocity along the horizontal direction. It is assumed that the road excitations of the left and right wheels are the same. The road excitations of the rear wheels are same as but delayed from the road excitations of the front wheels for a constant vehicle speed.

In the simulations, the following control methods are compared:

(1) The passive suspension system, which is referred to as passive mode.
(2) The active suspension system with the proposed control, which is referred to as controller I.
(3) The active suspension system with the traditional LESO-based feedback linearization control, which is referred to as controller II.

The simulation results are displayed in Figures 2 ~ 6. The heave, pitch, and roll displacements of the car body under different controllers for the bump road input are compared in Figure 2, where the gray dotted-line represents the response of the passive suspension system, the red solid-line represents the response of the active suspension system with controller II. The proposed controller I achieves the smallest amplitude, and all the displacements converge to zero in finite time. Roll displacement still appears in this case because $c \neq d$. The time histories of the heave, pitch and roll accelerations are illustrated in Figure 3. The active suspension systems with controller I can attenuate the

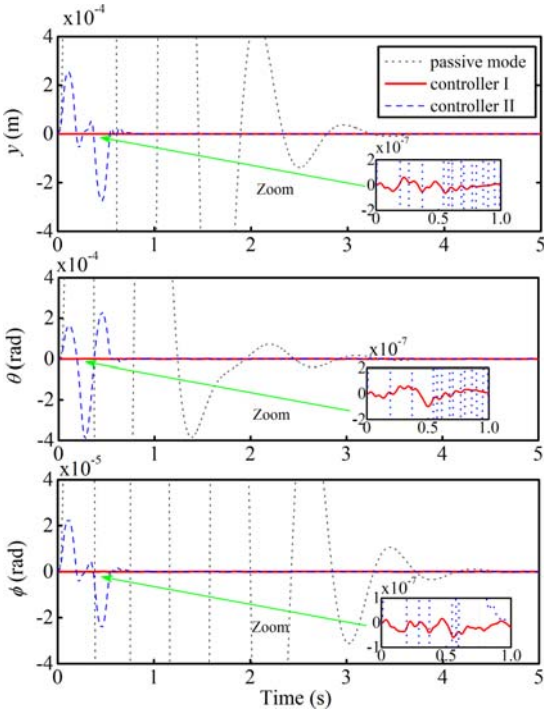

Figure 2. Heave, pitch, and roll displacements of the vehicle body for a bump road input.

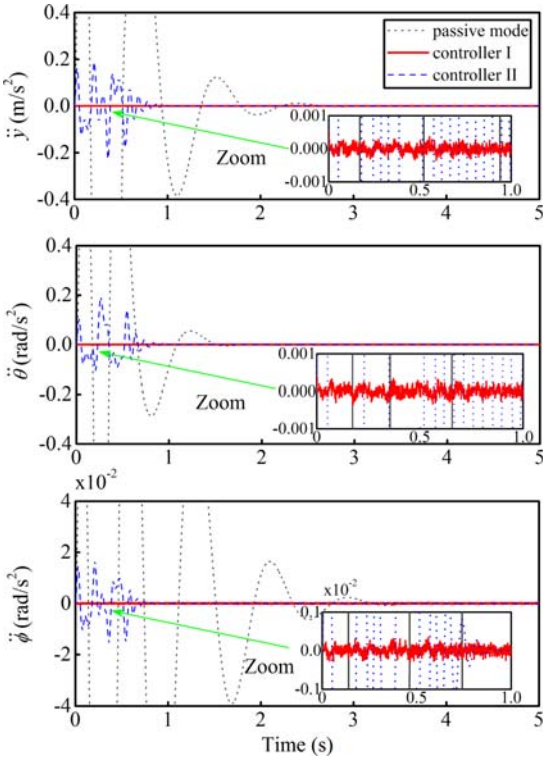

Figure 3. Comparison of the body acceleration with different controllers for a bump road input.

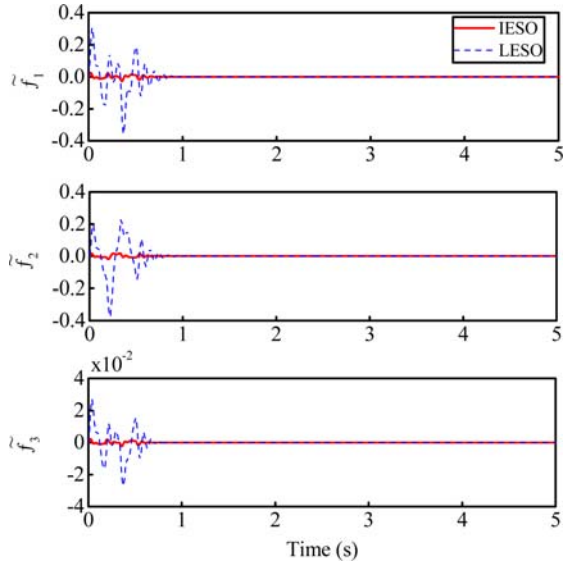

Figure 4. Estimation errors of the lumped uncertainty with different ESOs.

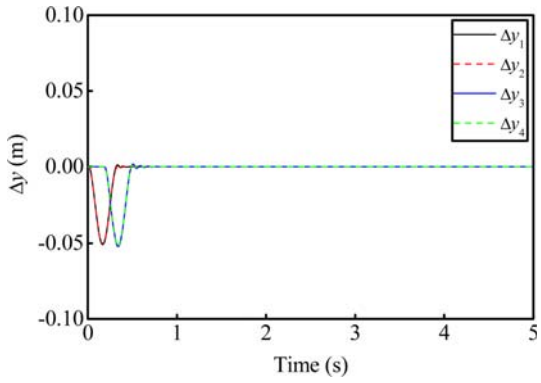

Figure 5. Suspension spaces of the active suspension systems with controller I.

accelerations more effectively than the active suspension systems with controller II, which implies that improved damping performance is achieved by the proposed controller.

To demonstrate the performances of the improved ESO, the estimate errors of the uncertainty f_i under different ESOs are given in Figure 4. The numerical results show that the improved extended-state observer (IESO) exhibits a faster convergence rate and a smaller peak value than the LESO for the same bandwidth parameter (ω_0 = 100). All the estimation errors converge to zero in approximately 0.85 s for the IESO and 1 s for the LESO. The biggest peak value of $f_1 - \hat{f}_1$ for the IESO is between 0.03 and − 0.03, while for LESO, the biggest peak value is between 0.4 and − 0.4. The suspension spaces and the actuator forces of the active suspension systems with controller I are plotted in Figures 5 and 6, respectively. The suspension spaces are all within a reasonable range, and the control forces are all smooth curves without chattering. These results verify the merits of the designed control scheme.

5.2. Simulation in Case 2 (Actuator faults present)

To further validate the finite-time stability of the proposed controller for the uncertain full-car active suspension with actuator faults, we assume the fault vector of the actuators is $\lambda = [0.5\ 0.6\ 0.5\ 0.6]^T$.

A continuous sine excitation is used in the following simulations, which can be expressed as

$$\begin{cases} y_{01}(t) = 0.01\sin(10\pi t) \\ y_{02}(t) = 0.01\sin(10\pi t) \\ y_{03}(t) = y_{01}\left(t - \frac{a+b}{V}\right) \\ y_{04}(t) = y_{02}\left(t - \frac{a+b}{V}\right) \end{cases} \tag{53}$$

where V = 15 m/s, and the excitation frequency is chosen as

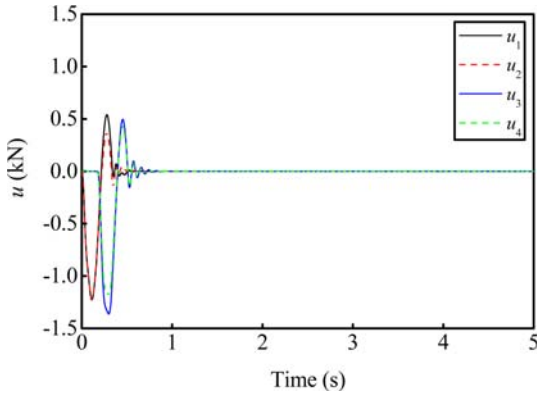

Figure 6. Actuator forces of the active suspension systems with controller I for bump road input.

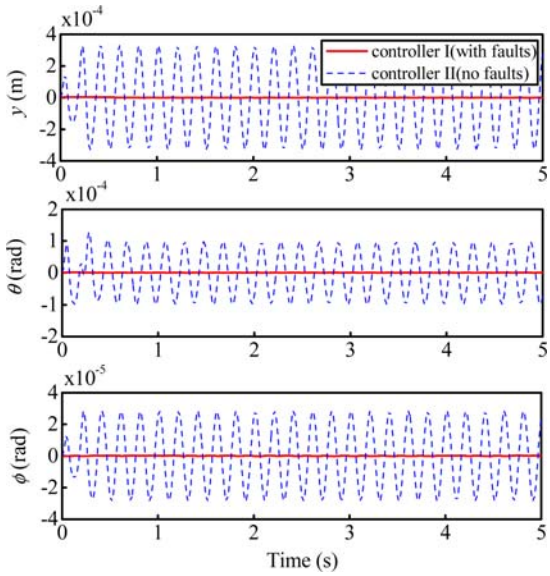

Figure 7. Heave, pitch, and roll displacements of the vehicle body for sinusoidal road input.

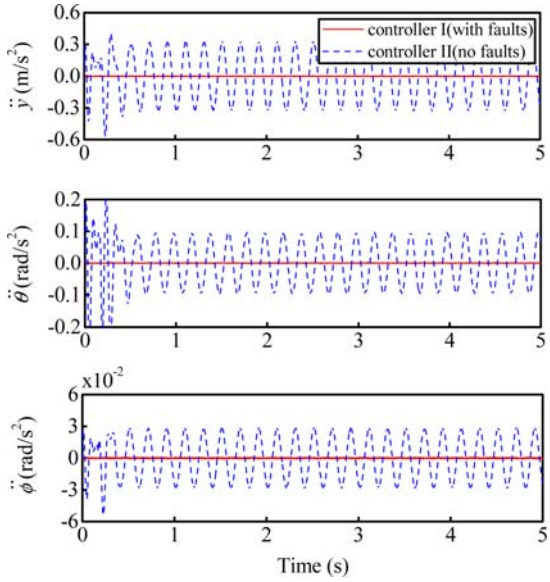

Figure 8. Comparison of the body acceleration under different controllers for sinusoidal road input.

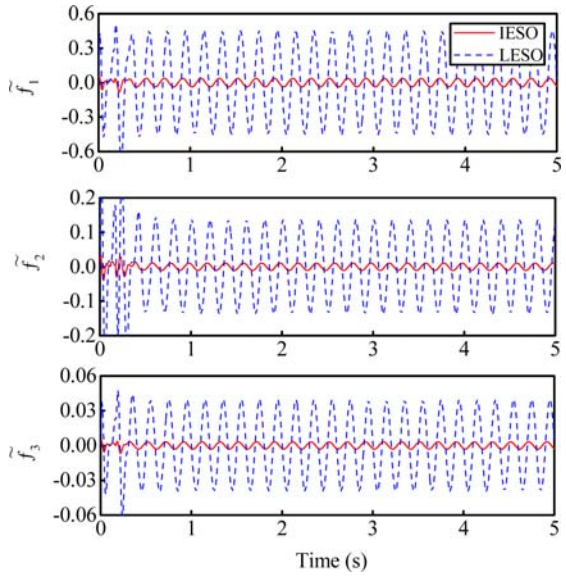

Figure 9. Estimation errors of the lumped uncertainty with different ESOs.

5 Hz, because the human body is more sensitive to vibrations in the 4 ~ 8 Hz range. This corresponds to a vehicle moving across a continuous bump and hole at a high speed.

Comparative results are shown in Figures 7 ~ 11. All the displacements and accelerations of the heave, pitch, and roll directions for the active suspension systems with controller I can be regulated to a given equilibrium in finite time under a continuous sine excitation, even with the actuator faults present, while the active suspension systems with controller II fails. According to Figure 9, the estimate errors of the IESO are one order of magnitude smaller than that those of the LESO, with values close to zero. The numerical results verify that the improved ESO is more effective for fast changing disturbances. Suspension spaces of the suspension systems with controller I under sine excitation are shown in Figure 10. The suspension spaces

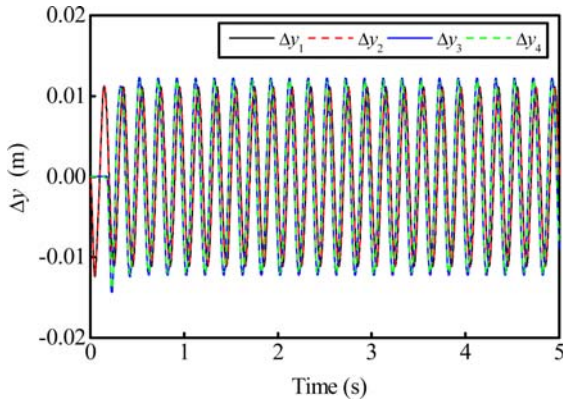

Figure 10. Suspension spaces of the active suspension systems with controller I.

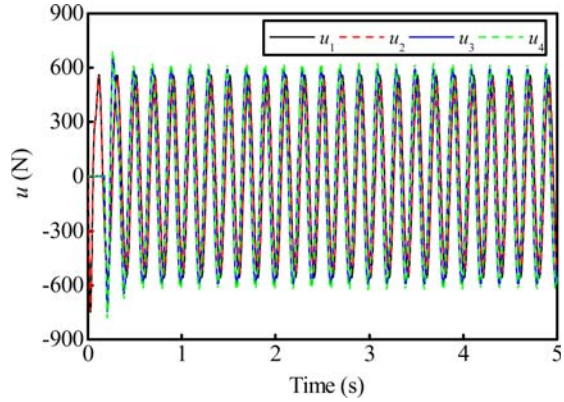

Figure 11. Actuator forces of the active suspension systems with controller I.

change within a reasonable range. As shown in Figure 11 all the control signals are absolutely continuous without chattering. The active disturbance rejection performance of the IESO decreases as the frequency of the disturbance increases. However, road disturbances mainly reside in the low frequency domain. Thus, the control scheme is effective and feasible.

6. CONCLUSION

A fault-tolerant-control scheme based on an ESO with finite-time convergent performance is presented to address the control problem of uncertain full-car active suspensions. To stabilize the heave, pitch, and roll displacements in a given equilibrium in finite time, a robust and absolutely continuous controller with non-singular terminal sliding mode is proposed for the control law synthesis. In addition, an improved extended state observer is employed to track the lumped uncertainty of the suspension systems. The novelty of this control scheme is that high-accuracy control performance can be achieved with minimal information of the model and a small number of sensors, even if actuator faults occur. As indicated by the numerical results, the proposed control scheme can achieve better control precision and a faster convergence rate than the traditional LESO-based feedback linearization control, and all the suspension requirements are improved in the proposed control.

ACKNOWLEDGEMENT–The work was supported by Qian-ke-he platform talent [2017]5789-11. The authors would like to thank the reviewers for their valuable suggestions.

REFERENCES

Ahmed, N. and Chen, M. (2018). Sliding mode control for quadrotor with disturbance observer. *Advances in Mechanical Engineering* **10**, **7**, 1–16.

Akbari, A. and Lohmann, B. (2010). Output feedback H_∞/

GH_2 preview control of active vehicle suspensions: A comparison study of LQG preview. *Vehicle System Dynamics: Int. J. Vehicle Mechanics and Mobility* **48**, **12**, 1475–1494.

Boker, A. M. and Khalil, H. K. (2013). Nonlinear observers comprising high-gain observers and extended Kalman filters. *Automatica* **49**, **12**, 3583–3590.

Brezas, P., Smith, M. C. and Hoult, W. (2015). A clipped-optimal control algorithm for semi-active vehicle suspensions: Theory and experimental evaluation. *Automatica*, **53**, 188–194.

Deshpande, V. S., Mohan, B., Shendge, P. D. and Phadke, S. B. (2014). Disturbance observer based sliding mode control of active suspension systems. *J. Sound and Vibration* **333**, **11**, 2281–2296.

Gao, H., Lam, J. and Wang, C. (2006). Multi-objective control of vehicle active suspension systems via load-dependent controllers. *J. Sound and Vibration* **290**, **3-5**, 654–675.

Gosiewski, Z. and Mystkowski, A. (2008). Robust control of active magnetic suspension: Analytical and experimental results. *Mechanical Systems and Signal Processing* **22**, **6**, 1297–1303.

Guo, B. and Zhao, Z. (2011). On the convergence of an extended state observer for nonlinear systems with uncertainty. *Systems & Control Letters* **60**, **6**, 420–430.

Hong, Y. (2002). Finite-time stabilization and stabilizability of a class of controllable systems. *Systems & Control Letters* **46**, **4**, 231–236.

Hong, Y., Xu, Y. and Huang, J. (2002). Finite-time control for robot manipulators. *Systems & Control Letters* **46**, **4**, 243–253.

Huang, B., Hsieh, C. Y., Golnaraghi, F. and Moallem, M. (2015a). Development and optimization of an energy-regenerative suspension system under stochastic road excitation. *J. Sound and Vibration*, **357**, 16–34.

Huang, Y. B., Na, J., Wu, X., Liu, X. Q. and Guo, Y. (2015b). Adaptive control of nonlinear uncertain active suspension systems with prescribed performance. *ISA Trans*., **54**, 145–155.

Karkoub, M. A. and Zribi, M. (2006). Active/Semi-active suspension control using magnetorheological actuators. *Int. J. Systems Science* **37**, **1**, 35–44.

Li, S., Yang, J., Chen, W. H. and Chen, X. (2012). Generalized extended state observer based control for systems with mismatched uncertainties. *IEEE Trans. Industrial Electronics* **59**, **12**, 4792–4802.

Lin, J. and Lian, R. J. (2011). Intelligent control of active suspension systems. *IEEE Trans. Industrial Electronics* **58**, **2**, 618–628.

Liu, S., Zhou, H., Luo, X. and Xiao, J. (2016). Adaptive sliding fault tolerant control for nonlinear uncertain active suspension systems. *J. Franklin Institute* **353**, **1**, 180–199.

Pan, H., Sun, W., Gao, H. and Yu, J. (2015b). Finite-time stabilization for vehicle active suspension systems with hard constraints. *IEEE Trans. Intelligent Transportation Systems* **16**, **5**, 2663–2672.

Pan, H., Sun, W., Gao, H., Hayat, T. and Alsaadi, F. (2015a). Nonlinear tracking control based on extended state observer for vehicle active suspensions with performance constraints. *Mechatronics*, **30**, 363–370.

Ran, M., Wang, Q. and Dong, C. (2016). Stabilization of a class of nonlinear systems with actuator saturation via active disturbance rejection control. *Automatica*, **63**, 302–310.

Sande, T. P. J., Gysen, B. L. J., Besselink, I. J. M., Paulides, J. J. H., Lomonova, E. A. and Nijmeijer, H. (2013). Robust control of an electromagnetic active suspension system: Simulations and measurements. *Mechatronics* **23**, **2**, 204–212.

Shao, X. and Wang, H. (2014). Sliding mode based trajectory linearization control for hypersonic reentry vehicle via extended disturbance observer. *ISA Trans*. **53**, **6**, 1771–1786.

Spelta, C., Previdi, F., Savaresi, S. M., Bolzern, P., Cutini, M., Bisaglia, C. and Bertinotti, S. A. (2011). Performance analysis of semi-active suspensions with control of variable damping and stiffness. *Vehicle System Dynamics: Int. J. Vehicle Mechanics and Mobility* **49**, **1-2**, 237–256.

Sun, W., Gao, H. and Kaynak, O. (2011). Finite frequency H_∞ control for vehicle active suspension systems. *IEEE Trans. Control Systems Technology* **19**, **2**, 416–422.

Sun, W., Gao, H. and Kaynak, O. (2013). Adaptive backstepping control for active suspension systems with hard constraints. *IEEE/ASME Trans. Mechatronics* **18**, **3**, 1072–1079.

Sun, W., Pan, H., Zhang, Y. and Gao, H. J. (2014). Multi-objective control for uncertain nonlinear active suspension systems. *Mechatronics* **24**, **4**, 318–327.

Unger, A., Schimmack, F., Lohmann, B. and Schwarz, R. (2013). Application of LQ-based semi-active suspension control in a vehicle. *Control Engineering Practice* **21**, **12**, 1841–1850.

Wang, G., Chadli, M., Chen, H. and Zhou, Z. (2019). Event-triggered control for active vehicle suspension systems with network-induced delays. *J. Franklin Institute* **356**, **1**, 147–172.

Wang, G., Chen, C. and Yu, S. (2017). Finite-time sliding mode tracking control for active suspension systems via extended super-twisting observer. *Proc. Institution of Mechanical Engineers, Part D: J. Systems and Control Engineering* **231**, **6**, 459–470.

Wang, R., Jing, H., Yan, F., Karimi, H. R. and Chen, N. (2015a). Optimization and finite-frequency H_∞ control of active suspensions in in-wheel motor driven electric ground vehicles. *J. Franklin Institute* **352**, **2**, 468–484.

Wang, R., Jing, H., Yan, F., Karimi, H. R. and Chen, N. (2015b). Robust fault-tolerant H_∞ control of active suspension systems with finite-frequency constraint. *Mechanical Systems and Signal Processing*, **62-63**, 341–

355.
Xiong, S., Wang, W., Liu, X., Chen, Z. and Wang, S. (2015). A novel extended state observer. *ISA Trans*., **58**, 309–317.
Yagiz, N. and Hacioglu, Y. (2008). Backstepping control of a vehicle with active suspensions. *Control Engineering Practice* **16**, **12**, 1457–1467.
Yao, J., Jiao, Z. and Ma, D. (2014). Adaptive robust control of DC motors with extended state observer. *IEEE Trans. Industrial Electronics* **61**, **7**, 3630–3637.
Youn, I., Khan, M. A., Uddin, N., Youn, E. and Tomizuka, M. (2017). Road disturbance estimation for the optimal preview control of an active suspension systems based ontracked vehicle model. *Int. J. Automotive Technology* **18**, **2**, 307–316.
Zhang, G., Cao, J. and Yu, F. (2012). Design of active and energy-regenerative controllers for DC-motor-based suspension. *Mechatronics* **22**, **8**, 1124–1134.
Zhang, J., Han, Z. and Huang, J. (2013). Homogeneous feedback design of differential inclusions based on control Lyapunov functions. *Communications in Nonlinear Science and Numerical Simulation* **18**, **10**, 2790–2800.
Zhang, Y., Zhang, X., Zhan, M., Guo, K., Zhao, F. and Liu, Z. (2015). Study on a novel hydraulic pumping regenerative suspension for vehicles. *J. Franklin Institute* **352**, **2**, 485–499.
Zhao, Z. and Guo, B. (2015). On active disturbance rejection control for nonlinear systems using time-varying gain. *European J. Control*, **23**, 62–70.
Zheng, Q., Dong, L., Lee, D. H. and Gao, Z. (2009). Active disturbance rejection control for MEMS gyroscopes. *IEEE Trans. Control Systems Technology* **17**, **6**, 1432–1438.